

Fractional Encoding of Harmonic Motions in MR Elastography

Jens Rump,¹ Dieter Klatt,¹ Jürgen Braun,² Carsten Warmuth,¹ and Ingolf Sack^{1*}

In MR elastography (MRE) shear waves are magnetically encoded by bipolar gradients that usually oscillate with the same frequency f_v as the mechanical vibration. As a result, both the repetition time (TR) and echo time (TE) of such an MRE sequence are greater than the vibration period $1/f_v$. This causes long acquisition times and considerable signal dephasing in tissue with short transverse relaxation times. Here we propose a reverse concept with $TR \leq 1/f_v$, which we call “fractional” MRE, i.e., only a fraction of one vibration cycle per TR, can be used for motion sensitization. The benefit of fractional MRE is twofold: 1) acquisition times in seconds can be achieved for a single-phase difference wave image, and 2) materials that combine low elasticity, high viscosity, and short T_2^* relaxation times show an increased phase-to-noise ratio (PNR). A twofold increase of the phase signal is predicted for liver-like materials. Volunteer studies performed in liver and biceps show the benefit of fractional MRE. Furthermore, we demonstrate the feasibility of the technique for in vivo myocardial MRE by visualizing transverse wave propagation in the interventricular septum (IVS). Magn Reson Med 57:388–395, 2007. © 2007 Wiley-Liss, Inc.

Key words: balanced SSFP; steady-state; elastography; liver; skeletal muscle; myocardium; interventricular septum

Manual palpation is a sensitive means of detecting pathologically altered tissue near the surface of the body. The sensitivity of this method is related to the resistance of soft tissue to shear forces, which varies by orders of magnitude in the human body (1,2). Accordingly, elastography techniques have been developed to quantify the shear elasticity of living human tissue based on soft-tissue imaging techniques, such as ultrasound or MRI, using either static mechanical compression or acoustic strain waves (3–9). Since the acoustic approach in MR elastography (MRE) has made rapid progress in the last few years, it is now possible to examine the elasticity of tissue that is not palpable from the body surface. Dynamic MRE can map spatial and temporal shear wave fields that depend on heterogeneity, anisotropy, and nonlinearity of the elasticity (10–17).

Although pilot studies demonstrated the potential of MRE, it has remained a relatively slow technique compared to the rapid acquisition schemes of other flow- or motion-quantifying MRI methods (18–21). The extended

time consumption of conventional MRE scans is due to the duration of bipolar gradients used to sensitize the sequence to slow mechanical vibration cycles (usually >5 ms, corresponding to vibration frequencies of $f_v < 200$ Hz). This frequency range is compelled by the high viscosity of most soft tissues that results in a rapid damping of the shear wave amplitude with the penetration distance (22). Current MRE methods encode the motion by oscillating gradients with a minimum duration of one vibration cycle. Thus, the repetition time (TR) of an MRE sequence is always greater than $1/f_v$.

In this work we propose the use of low-frequency shear vibrations with vibration cycles longer than the TR of the MRI sequence ($TR \leq 1/f_v$). As a trade-off, only a fraction of one motion cycle can be magnetically encoded, and thus the phase difference signal is smaller. However, it will be shown that for soft and viscous materials with short transverse relaxation times this loss is more than compensated for by an increased signal resulting from reduced transverse relaxation. The short echo times (TEs) that are achievable with fractional motion encoding also enable MRE to be performed in the presence of blood flow or heart motion, which permits in vivo examinations of myocardial elasticity.

Although fractional motion encoding is feasible with any type of signal readout, all experiments in this study are based on a balanced steady-state free precession (bSSFP) experiment (i.e., all gradients are fully refocused within one TR) (23–27). Bieri et al. (28) recently introduced bSSFP-MRE based on intrinsic motion sensitization by readout gradients. The authors proposed the use of three half-motion cycles in one SSFP-TR to produce an oscillating steady state with acquisition of two images corresponding to the alternating offset of motion phase. In the present study, an extra motion sensitization gradient is employed such that the length of the SSFP-TR is adapted to one, one-half, or one-quarter vibration cycle. In the latter two cases, where $TR < 1/f_v$, an alternating steady-state is produced as described in Ref. 28.

In the following text we will first derive a theoretical expression for the motion phase in fractional MRE that accounts for NMR and viscoelastic parameters. The MRE phase signal for liver- and muscle-like materials is predicted based on this equation, and experimental parameters are proposed and validated by in vivo experiments on human biceps and liver. Furthermore, the feasibility of fractional MRE for detecting slow shear vibrations in the human heart is demonstrated on the interventricular septum (IVS) of a volunteer.

THEORY

bSSFP sequences require short TRs to minimize the effect of field inhomogeneities on the signal evolution that lead

¹Department of Radiology, Charité-Universitätsmedizin Berlin, Berlin, Germany.

²Institute of Medical Informatics, Charité-Universitätsmedizin Berlin, Berlin, Germany.

Grant sponsor: German Research Foundation; Grant number: Sa/901-2.

*Correspondence to: Ingolf Sack, Ph.D., Department of Radiology, Charité-Universitätsmedizin Berlin, Charitéplatz 1, 10117 Berlin, Germany. E-mail: ingolf.sack@charite.de

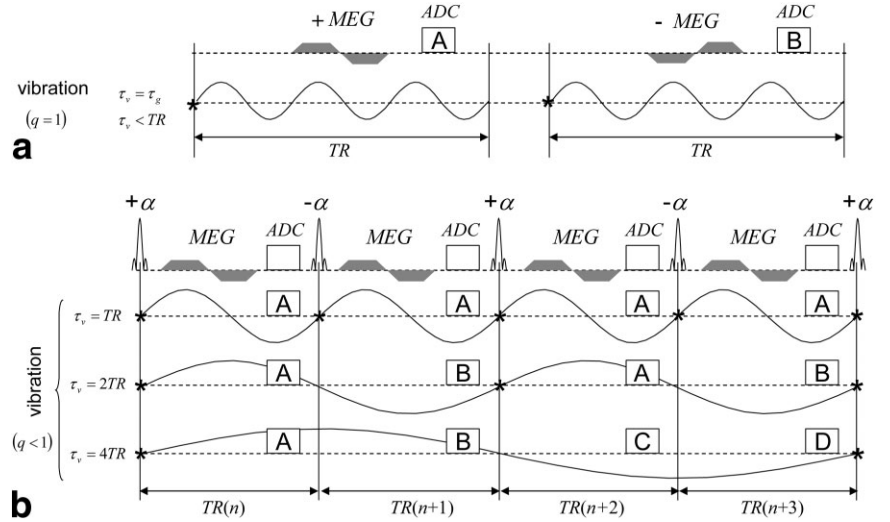
Received 2 March 2006; revised 29 September 2006; accepted 31 October 2006.

DOI 10.1002/mrm.21152

Published online in Wiley InterScience (www.interscience.wiley.com).

© 2007 Wiley-Liss, Inc.

FIG. 1. **a**: Sketch of a conventional MRE experiment using equal periods of bipolar motion-encoding gradients and vibration. The asterisks indicate the wave generator trigger. The gradient polarity is toggled in consecutive experiments with data sampling A and B, yielding two sets of data that give an inverse motion phase contrast. **b**: Three types of fractional MRE. The length of one vibration period τ_v is matched to N TRs with $N = 1, 2$, and 4 . For $N = 1$, a second experiment with reversed MEG polarity is required in order to compute $\Delta\phi$, just as in part a. For $N = 2$, two phase images for subtraction are acquired in subsequent TRs, while with $N = 4$, four sets of data are sampled during the periods A, B, C, and D.



to banding artifacts in off-resonance regions (29,30). Motion sensitization by extra bipolar gradients prolongs the minimum achievable TR and can thus compromise bSSFP image quality. As stated above, in vivo MRE often necessitates the application of shear waves in the low audio range, which can easily extend TR above 20 ms using conventional motion encoding by matching one bipolar gradient period (τ_g) with one vibration cycle (τ_v), i.e., $\tau_g = \tau_v$ (Fig. 1a). To combine a short TR and low vibration frequencies in SSFP-MRE, one vibration cycle must exceed τ_g in such a manner that τ_v is matched to integer TRs:

$$\tau_v = N \cdot TR; (N = 1, 2, 3, \dots) \quad \text{and} \quad q = \frac{\tau_g}{\tau_v} < 1. \quad [1]$$

The ratio q is a measure of the vibration cycle fraction used for motion encoding. In conventional MRE, q equals one, since the vibration frequency f_v is bound not to the TR but to $1/\tau_g$. In contrast, in fractional encoding, q is always smaller than one, i.e., only fractions of the vibration cycles are used for motion encoding.

Phase Signal Evolution

We considered spins in a steady state of mechanical vibration. The spins oscillate harmonically with maximum amplitude u and phase $2\pi f_v t + \theta$, where θ is a constant phase offset determined by the onset of the wave generator and the location of the vibrating particles relative to the wave source.

The phase that accumulates during the n -th TR caused by harmonic motion can then be calculated as:

$$\phi_n = \gamma u \int_{(n-1)TR}^{nTR} G(t) \sin(2\pi f_v t + \theta) dt, \quad [2]$$

where γ is the gyromagnetic ratio of protons, and $G(t)$ represents any gradient component in the direction of the particle deflection u . Figure 2 shows the vibration-induced phase shift that is due to a single-period, bipolar, trapezoidal motion encoding gradient (MEG), as used in the exper-

iments here. It illustrates that $N = 1$ results in a constant phase shift, yielding the well-known misregistration artifact of spins moving at a constant velocity. However, if $N > 1$, interference between TR and vibration is produced, causing ϕ_n to oscillate (31). In the particular case of $N = 2$, the spin phase is flipped at each TR. This alternation of ϕ_n can be exploited to split the lines in k -space into two separate images A and B, corresponding to ϕ_n and ϕ_{n+1} (28). In general, each N^{th} TR can be used to form an image that results in a series of N images representing different phase offsets between vibration and motion-encoding gradients.

Since in the steady state ϕ_n is periodic in $N \cdot TR$, we further consider a spin phase $\phi = \phi_n = \phi_{n+N}$ in the following. Furthermore, it is assumed that harmonic gradients are used for motion encoding, where the MEG is

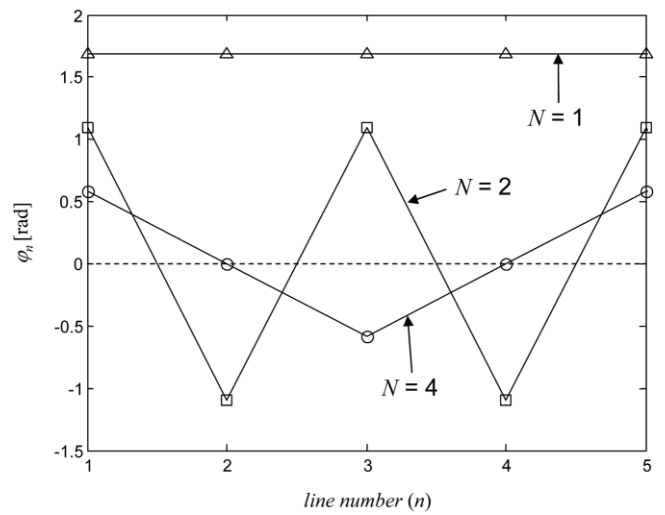


FIG. 2. Steady-state spin phase ϕ_n calculated by using Eq. [2] with MEG and vibrations as schematically represented in Fig. 1b. The dashed graph represents absence of motion. The vibration phase θ was chosen so that ϕ_1 is at a maximum. Further simulation parameters: $\tau_g = 6.7$ ms, $g = 35$ mT/m, slew rate = 120 mT/m/ms, $u = 40$ μ m, $f_v = 100$ Hz (Δ), 50 Hz (\square), and 25 Hz (\circ).

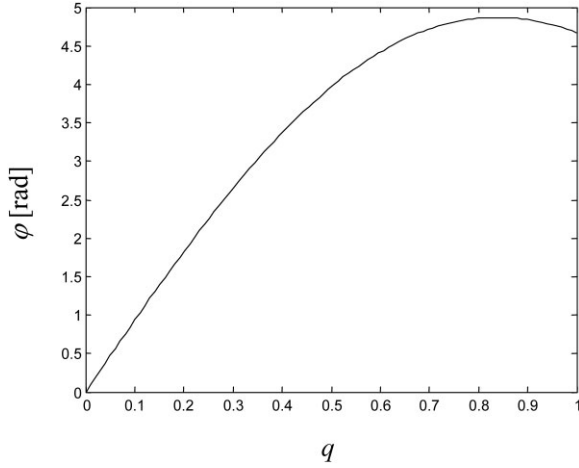


FIG. 3. Encoded phase signal φ without relaxation calculated using Eq. [3]. The maximum attainable phase shift is approached with vibration frequencies $f_v < f_g$. Simulation parameters: $g = 35$ mT/m, $u = 100$ μ m.

given by $G(t) = g\sin(2\pi f_g t)$, with g and f_g being the amplitude and frequency of the sinusoid, respectively. The number of gradient cycles (n_g) equals one, which is the shortest possible MEG at a given f_g . Relaxation is not considered. Equation [2] can then be solved analytically for the maximum phase shift φ originating from the motion-encoding gradients:

$$\varphi = \frac{\gamma g u \tau_g}{\pi} \frac{\sin(\pi q)}{1 - q^2}, \quad \theta = \pi(1 - q), \quad n_g = 1, \quad [3]$$

which is achieved at $\theta = \pi(1 - q)$. In MRE experiments, when two phase images are acquired with either toggled MEGs or inverse wave amplitudes, the phase difference $\Delta\varphi$ is twice that value (e.g., $\Delta\varphi = A - B$ with $N = 1$ or 2 ; $\Delta\varphi = A - C$; or $\Delta\varphi = B - D$ with $N = 4$; see Fig. 1). Within the confines of conventional MRE ($q = 1$), Eq. [3] converges to $\varphi = \gamma g u \tau_g / 2$. Interestingly, Eq. [3] predicts the maximum of $\Delta\varphi$ at $f_v < f_g$, and not at matching frequencies. A third-order expansion of φ around $q = 1$ yields $q = (2\pi^2 - 6)/(2\pi^2 - 3)$ for the approximated position of the maximum phase (see Fig. 3). Thus, applying $f_v \approx 0.82f_g$ results in a slightly higher phase response than that achieved in conventional MRE with single bipolar gradients ($n_g = 1$).

Phase-to-Noise Ratio (PNR) in MRE

To derive a relationship between the NMR parameters and mechanical properties of the investigated material, we consider the location (X) of a vibrating isochromat at $X = c/f_v$, where c is the shear wave speed in the material. As such, X is equal to one shear wavelength, which in the following is regarded as a reference length of the desired penetration depth of the shear waves. The wave amplitudes will decrease by a monoexponential function $u = u_0 \exp(-\Gamma X)$ with the damping coefficient Γ and deflection amplitude u_0 at $X = 0$. Voigt's model of a viscoelastic

solid (1) can be employed to derive the functions of c and Γ on the vibration frequency f_v (32,33):

$$c = \sqrt{\frac{2}{\rho} \frac{\Theta}{\sqrt{\Theta} + \mu}}; \quad \Gamma = 2\pi f_v \sqrt{\frac{\rho}{2} \frac{\sqrt{\Theta} - \mu}{\Theta}} \quad [4]$$

$$\text{with } \Theta = \mu^2 + (2\pi f_v \eta)^2,$$

where μ and η denote the shear modulus and viscosity, respectively, and ρ is the material's density. Using this model, the mechanical deflection at one wavelength distance from the tissue boundary reads:

$$u = u_0 \exp\left(-\frac{4\pi^2 f_v \eta}{\mu + \sqrt{\Theta}}\right) \quad [5a]$$

$$\approx u_0 \exp\left(-\frac{2\pi^2 f_v \eta}{\mu}\right) \quad \mu^2 \gg (2\pi f_v \eta)^2. \quad [5b]$$

Equation [5b] is an approximation, which is useful for obtaining an analytical estimation of the optimum encoding time in fractional MRE. It applies with good accuracy to the viscoelastic parameter range explored by MRE of liver or skeletal muscle (e.g., using some typical viscoelastic values of $\mu = 5$ kPa and $\eta = 2$ Pas, as given in Ref. 34), and yields with $f_v = 100$ Hz an elasticity term μ^2 that is about 16 times greater than the viscous term $[2\pi f_v \eta]^2$.

To account for spin dephasing during the time of motion encoding (τ_g), we relate the PNR to the signal-to-noise ratio (SNR) of a magnitude image (35):

$$PNR \propto \frac{2\varphi}{\pi} SNR_0 \exp(-\tau_g/T_2^*), \quad [6]$$

where SNR_0 represents the SNR for a sequence without MEG, i.e., at $\tau_g = 0$. In SSFP-sequences SNR_0 is also flip-angle-dependent and has to be optimized for each investigated material and TR (35). In the following, SNR_0 is assumed to be constant for each material and SNR decreases due to T_2^* , which is experimentally determined by measuring the SNR by an increasing τ_g . The elastography equation combines Eqs. [3], [5], and [6]. A simplified expression is obtained by using Eq. [5b]:

$$PNR \propto \frac{2\gamma g \tau_g}{\pi^2} \frac{\sin(\pi q)}{1 - q^2} SNR_0 u_0 \exp\left(-\tau_g/T_2^* - \frac{2\pi^2 q \eta}{\tau_g \mu}\right), \quad [7]$$

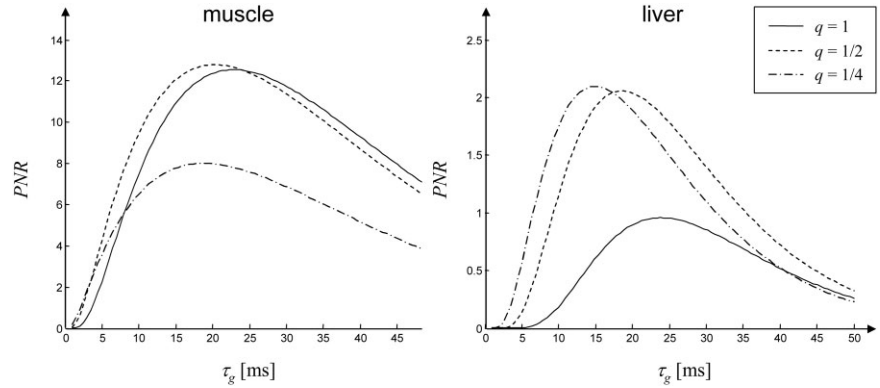
which has its maximum at

$$\tau_g^{opt} = \frac{1}{2} T_2^* + \frac{1}{2} \sqrt{T_2^{*2} + 8\pi^2 T_2^* q \frac{\eta}{\mu}}. \quad [8]$$

Without viscosity, the highest PNR in MRE is approached when the optimum MEG duration (τ_g^{opt}) equals T_2^* (36), whereas τ_g^{opt} is prolonged beyond T_2^* when η is greater than zero.

Figure 4 shows the predicted PNR in fractional MRE for two materials. It is apparent that the combination of low μ , high η , and short T_2^* , as found in the liver, strongly sup-

FIG. 4. Calculated PNR in fractional MRE according to Eq. [7] of two viscoelastic materials modeling muscle ($\mu = 5000$ Pa, $\eta = 2$ Pas, $T_2^* = 17$ ms) and human liver ($\mu = 2000$ Pa, $\eta = 4$ Pas, $T_2^* = 9$ ms). Further simulation parameters: $u_0 = 100$ μm ; $g = 35$ mT/m, $\text{SNR}_0 = 10$.



ports fractional motion encoding with lower q -values. For example, using the parameters given in the caption of Fig. 4, the maximum PNR (at $\tau_g = \tau_g^{opt}$) is more than doubled when $q = 1/4$ or $1/2$ (PNR = 2.1) is employed instead of the conventional limit of $q = 1$ (PNR = 1.0). In muscle, $q = 1/4$ (PNR = 8.0) causes a 1.5-fold decrease of the PNR compared to $q = 1/2$ (PNR = 12.8) or $q = 1$ (PNR = 12.5). The figure changes when a specific vibration frequency is desired. For example, with $f_v = 50$ Hz $q = 1/4$ yields a lower PNR in both materials examined, while $q = 1/2$ increases the PNR in liver about 25% from 0.9 to 1.2 compared to $q = 1$. This is in contrast to muscle tissue, where $q = 1/2$ and $f_v = 50$ Hz yield lower PNRs than $q > 1/2$. Since the vibration frequency in SSFP-MRE is constrained by the sequence TR, only certain parameter combinations are experimentally allowed. By neglecting the time of the imaging gradients (i.e., $\tau_v = N\tau_g$) q equals $1/N$. Thus the given scenarios in Fig. 4 apply to the vibration schemes of $N = 1, 2$, and 4 as shown in Fig. 1.

Experiments

All MRE experiments were performed on a 1.5 T scanner (Magnetom Sonata; Siemens, Erlangen, Germany). For the MRE image acquisition, we sensitized a conventional bSSFP sequence to motion by inserting a trapezoidal, bipolar gradient with variable direction, frequency, and amplitude between the phase-encoding and readout gradients. We locked the vibration phase to the MR image acquisition by triggering the wave generator at the start of each N^{th} TR cycle, as indicated in Fig. 1.

Biceps

Fractional MRE with $N = 1$ was applied to the human biceps using $f_g = 200$ Hz, TR = 8.34 ms, and $f_v = 120$ Hz ($q = 0.6$) in a first experiment, and $f_g = 100$ Hz, TR = 13.34 ms, and $f_v = 75$ Hz ($q = 0.75$) in a second experiment. Twenty wave images with alternating motion sensitization were acquired to produce 10 phase contrast images $\Delta\phi$. The wave trigger was shifted 10 times to cycle θ from $\pi/5$ to 2π . The acquisition of single images was repeated after 2.5 s, yielding a total measuring time of 50 s. Further sequence parameters were $g = 20$ mT/m along slice selection, FOV = 250 mm, matrix = 128×128 , slice thickness = 5 mm, $\alpha = \pm 50^\circ$, and coronal image plane through the long axis of the muscle. Mechanical excitation

of the biceps of a 33-year-old healthy male volunteer was achieved using an electromotive rocker unit as described in Ref. 37. To derive the elastic parameters, we applied shear-wave group-velocity inversion based on an automatic detection of wavelengths along rays (34). Tolerance margins were determined by the standard deviation (SD) of data obtained from the same subject in eight different sessions. We deduced T_2^* by fitting a monoexponential curve to the mean signal decay in the muscle measured in 12 experiments by increasing τ_g from 0 to 20 ms.

Liver

Two in vivo liver experiments were run with TRs of 9.85 and 13.2 ms corresponding to $f_v = 51$ Hz, $f_g = 150$ Hz, $N = 2$ ($q = 0.34$) and $f_v = 76$ Hz, $f_g = 100$ Hz, $N = 1$ ($q = 0.76$), respectively. Twenty wave images were acquired and either k -space reordering for reconstructing images A and B ($N = 2$) or an inversed amplitude of the MEG ($N = 1$) was applied so that 10 phase difference wave images $\Delta\phi$ were reconstructed, representing a full cycle of θ . We synchronized the acquisition with respiration by sampling five images during one breath-hold of 16.6 s in a total of four breath-holds. Further parameters were $g = 35$ mT/m along the direction of slice selection, FOV = 300×244 mm, matrix = 128×104 (resulting in approximately 13 and 10 pixels per shear wavelengths with $f_v = 50$ and 75 Hz, respectively), slice thickness = 10 mm, and $\alpha = \pm 50^\circ$. Transversal slices were positioned at the center of the liver of a 34-year-old healthy male volunteer. For mechanical excitation, one end of a transducer rod was mounted on a vibrating loudspeaker with the other end attached to the body's surface in the vicinity of the lower tip of the liver (38). The data were processed by extracting the first harmonic vibration as a complex wave image from the Fourier space at f_v (10). The complex data were fed into a linear inversion program based on an algebraic inversion of the wave equation including viscosity (33). Off-resonance effects on the motion sensitivity (28) that caused biases of the elastic modulus were found to be unimportant in the tolerance margins of our inversion algorithm. The error of the spatially averaged shear modulus was determined by the SD of seven experiments performed in the same volunteer on different days. The viscosity of the liver was estimated by the dispersion function of the wave speed at $f_v = 51$ and 76 Hz (Eq. [5]). T_2^* of liver was estimated in a

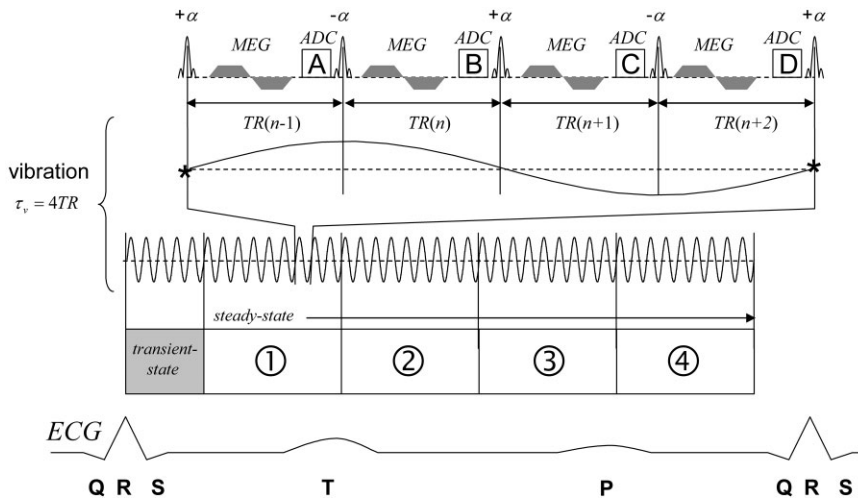


FIG. 5. Scheme of the myocardial MRE sequence with $N = 4$. The asterisks indicate the temporal position of a wave trigger. Nine vibration cycles were sampled in each cardiac phase (phases 1–4). The first five cycles or 20 RF excitations were skipped to reach the steady state.

manner similar to that described for muscle, but with τ_g ranging from 0 to 16.6 ms.

Heart

In vivo myocardial bSSFP-MRE was applied using $f_g = 500$ Hz and $f_v = 48.5$ Hz ($N = 4$, $q = 0.1$). These parameters resulted in a sequence TR of 5.2 ms, which was empirically found as a trade-off between motion-encoding efficiency and phase artifacts due to cardiac motion. The sequence timing relative to the ECG signal is shown in Fig. 5. Nine phase-encoding steps per cardiac cycle were measured for each of the interleaved k -space data A , B , C , and D , and one line in k -space was oversampled for reconstruction purposes. The choice of 36 lines representing a 187-ms imaging window allowed for four distinct phases of the cardiac cycle (labeled as phases 1–4 in Fig. 5). Eight heartbeats were needed to acquire the complete k -space of the phase difference images calculated by $\Delta\phi_1 = A - C$ and $\Delta\phi_2 = B - D$. The resulting phase difference maps were combined to a complex quantity $\Delta\phi = \Delta\phi_1 + i\Delta\phi_2$ based on the $\pi/2$ shift of the vibration phase between $\Delta\phi_1$ and $\Delta\phi_2$. The wave trigger was shifted 16 times with an increment $\Delta\theta = 1/8 \pi$. Four breath-holds of a 32-heartbeat duration were required to collect all of the data. Further acquisition parameters were $g = 30$ mT/m in the direction of slice selection, FOV = 400 mm, matrix = 128×64 , slice thickness = 5 mm, and $\alpha = \pm 50^\circ$. The image plane was aligned with the IVS. Vibrations of a loudspeaker were fed into a transducer rod attached to the chest of a healthy 36-year-old male volunteer. The vibration level was adjusted to produce low to moderate forces as assessed by the subjective impression of the volunteer. The wave data of each of the four acquired complex cardiac phases were temporally Fourier-filtered to separate the main vibration component at excitation frequency. The experiments were repeated four times on different days in the same volunteer.

RESULTS

Biceps

T_2^* and SNR_0 of bSSFP on muscle were measured with 17 ± 2 ms and 37 ± 2 , respectively. Using these parameters

together with $u_0 = 200 \mu\text{m}$, $\mu = 5$ kPa, and $\eta = 2$ Pas, Eq. [7] predicts an increase in PNR by a factor of 2.3 (from 30.1 to 70) when f_v is decreased from 120 Hz ($\tau_g = 5$ ms, $q = 0.6$) to 75 Hz ($\tau_g = 10$ ms, $q = 0.75$). The experimental consequence is demonstrated in Fig. 6: While the phase signal does not exceed $\pm\pi$ with a 120-Hz vibration frequency, aliasing of ϕ is produced with 75 Hz vibrations. Additionally, signal deteriorations are visible in the magnitude image of Fig. 6b at positions, where ϕ approaches $\pm\pi$. This effect is seen in bSSFP-MRE as a vibration-induced banding similar to field inhomogeneity-induced signal dephasing (29). The larger phase response in Fig. 6b is caused by increased mechanical deflection (from $50 \mu\text{m}$ to $150 \mu\text{m}$) combined with a higher encoding efficiency ($\approx 9\%$). While the first is a result of viscosity, the higher sensitivity of the sequence to the induced motion is caused by $q = 0.75$, which is in closer proximity to the position of the maximum of ϕ , as shown in Fig. 3. The wave pattern in the biceps show anisotropic wave propagation with $c = 2.27 \pm 0.19$ m/s and 5.28 ± 0.45 m/s for the wave speeds perpendicular and parallel to the muscle fibers. A dispersion of the measured wave speeds due to viscosity was not found, and viscosity was thus estimated to be in the range of 2 Pas, causing an error of the shear moduli below the experimental accuracy. Accordingly, shear moduli were derived from the perpendicular and parallel wave speeds with 5.2 ± 0.9 kPa and 28.1 ± 4.8 kPa, respectively, assuming a tissue density of 1000 kg/m^3 .

Liver

T_2^* and SNR_0 were determined with 9 ± 1 ms and 11 ± 1 . Using these values in combination with $u_0 = 100 \mu\text{m}$, $\mu = 2$ kPa and $\eta = 4$ Pas, Eq. [7] yields an increase in PNR from 0.1 to 0.9 by decreasing the vibration frequency from 76 Hz ($q = 0.76$, $N = 1$) to 51 Hz ($q = 0.34$, $N = 2$), as indicated by in vivo MRE experiments of the human liver (Fig. 7). In those experiments the SNR_0 of the reference experiment (Fig. 7a) decreased to approximately 3.5 (Fig. 7b) and 2.5 (Fig. 7c) due to the insertion of the motion sensitization gradient. However, the magnitude signal was sufficiently high for an evaluation of the phase signal. The maximum deflection amplitude was $80 \mu\text{m}$ with $f_v = 50$ Hz and $20 \mu\text{m}$ with $f_v = 75$ Hz. The wave data revealed a wave speed c at $f_v = 0$ (i.e., corrected for viscosity) of 1.55 ± 0.13

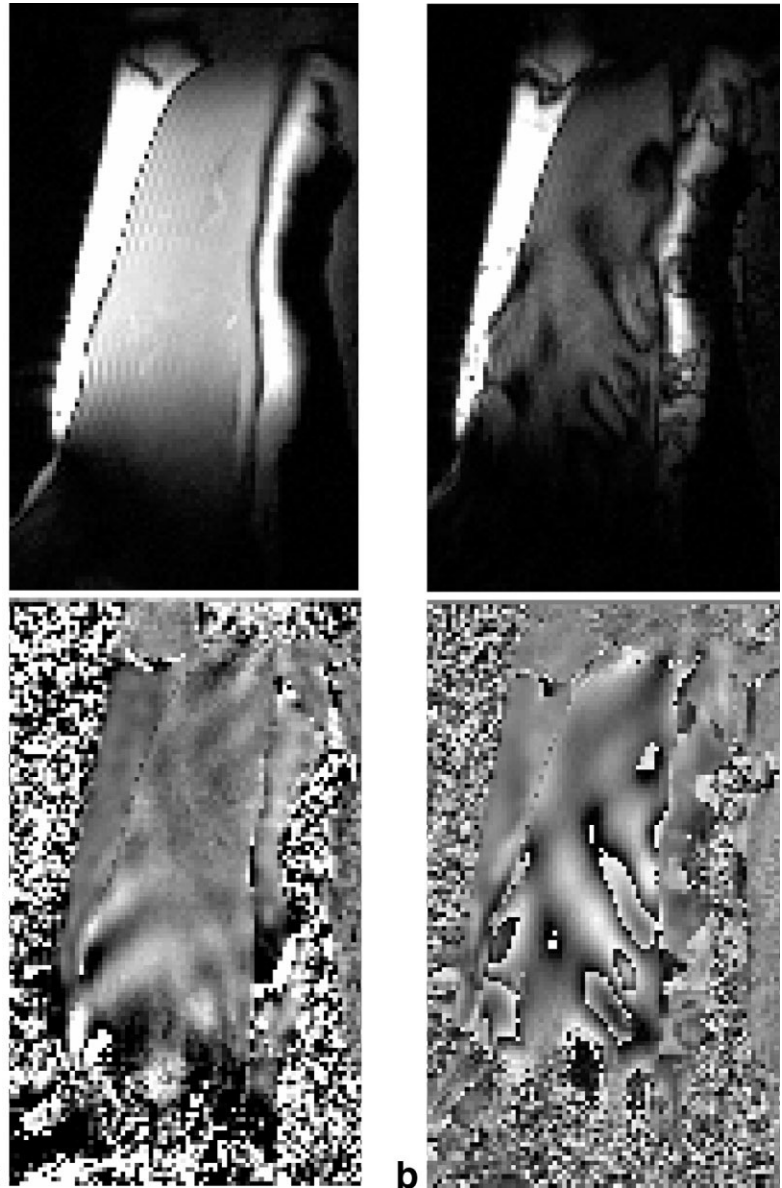


FIG. 6. bSSFP-MRE experiments on human biceps using (a) 120-Hz and (b) 75-Hz shear wave excitation with one vibration cycle per TR ($N = 1$). Magnitude images are shown on top, and normalized phase difference images are shown at the bottom. In b signal voids occur due to large-deflection-amplitude-related $\pm\pi$ phase accumulation per TR.

m/s and a corresponding shear modulus of 2.66 ± 0.48 kPa, assuming a liver tissue density of 1100 kg/m^3 (39). The viscosity estimated from the dispersion of the wave speeds at 50 Hz and 75 Hz was 4 ± 1 Pas.

Heart

Figure 8 demonstrates the feasibility of fractional MRE for detecting shear waves in the living human heart. Using cine bSSFP-MRI we found that the IVS largely remains within the image plane throughout the entire heart cycle. The position of the IVS at the start and end of each fractional MRE image acquisition is marked in Fig. 8a. The consecutively acquired phase difference images with 180-ms temporal resolution (phases 1–4) displayed in Fig. 8b show a transverse wave with normal propagation from the apex toward the aortic valve. The maximum deflection amplitude was estimated at $40 \mu\text{m}$ (without accounting for phase shifts due to the imaging gradients). Without vibra-

tions, no phase signal was obtained after the phase images $A-C$ and $B-D$ were subtracted. 3D animations provided by request from the authors illustrate the externally enforced vibrations of the segmented IVS at different cardiac phases. The animations were assembled from 16 frames displaying a calculated increment of $1/8\pi$ of the propagating wave phase. The septum is shown without surrounding tissue from a perspective view of 30° in-plane rotation and a 15° latitude tilt. The file names phase1.avi, phase2.avi, phase3.avi, and phase4.avi correspond to the time resolution during the cardiac cycle shown in Figs. 5 and 8. A comparison of the IVS vibrations indicates differences in the appearance of the waves at different cardiac phases.

The wave speed was one-dimensionally estimated by profiles along the wave normals indicated by the arrows in Fig. 8b. It was found that in all four phases of the cardiac cycle the detected wave propagates with a similar speed of 2.5 ± 0.4 m/s.

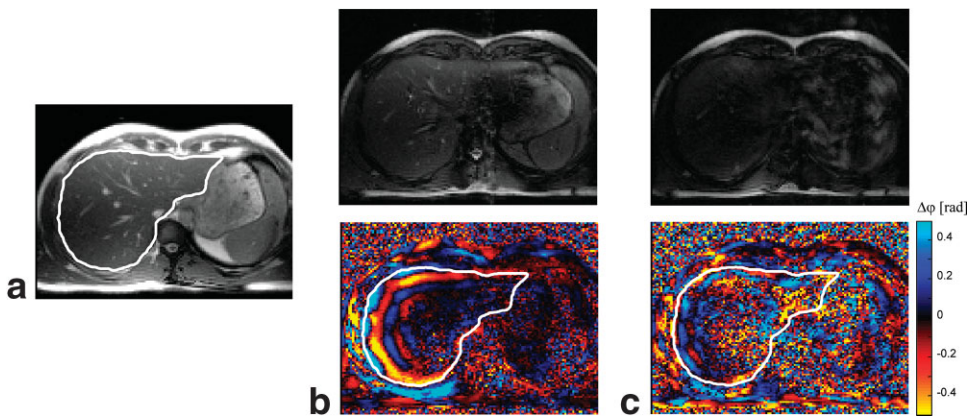


FIG. 7. In vivo bSSFP-MRE experiments in human liver. **a**: Reference bSSFP image acquired in a transversal plane without applying motion-sensitizing gradients. Also shown are bSSFP-MRE experiments at the same image slice position with **(b)** $f_v = 51$ Hz and $N = 2$, and **(c)** $f_v = 76$ Hz and $N = 1$.

DISCUSSION

This study demonstrates that fractional motion encoding improves the PNR in MRE of human liver and enables the measurement of externally induced vibrations in the myocardium. The main benefit of fractional motion encoding is that it reduces spin dephasing prior to the signal readout. To achieve that goal, other investigators proposed using the readout gradients for motion sensitization, which allows a match of τ_g and τ_v (28,40,41). However, since in that approach the sensitivity of the sequence to motion is dependent on the receiver bandwidth, the need for high SNR decreases the φ and thus the PNR. Additionally, only in-plane motions can be captured, which limits the applicability of MRE if specific wave field components have to be acquired.

The benefit of using only fractions of vibration cycles for motion encoding is derived from Eq. [7], which combines viscoelasticity and T_2^* -spin dephasing but does not account for TR-dependent steady-state perturbations. There-

fore, in general one should choose a shorter MEG in bSSFP-MRE than the one predicted by τ_g^{opt} (Eq. [8]). However, the proposed parameter combinations of f_v and N represent experimentally suitable values that may change when other sequence protocols or acoustic drivers are used.

The reproducibility of our data was tested in several follow-up studies performed on different days. It was found that the location of the actuator plays an important role in producing reproducible wave patterns in the biceps, liver, and heart. For example, in myocardial MRE, strong vibrations of the chest can cause a dominating rigid translation of the IVS that blinds out weak shear deflections. The optimization of the actuator mechanics in myocardial MRE is still being developed. The determined wave speed of 2.5 ± 0.4 m/s for all phases of the cardiac cycle is a preliminary result. Employing a simple plate model of wave motions in the IVS indicates a strong de-

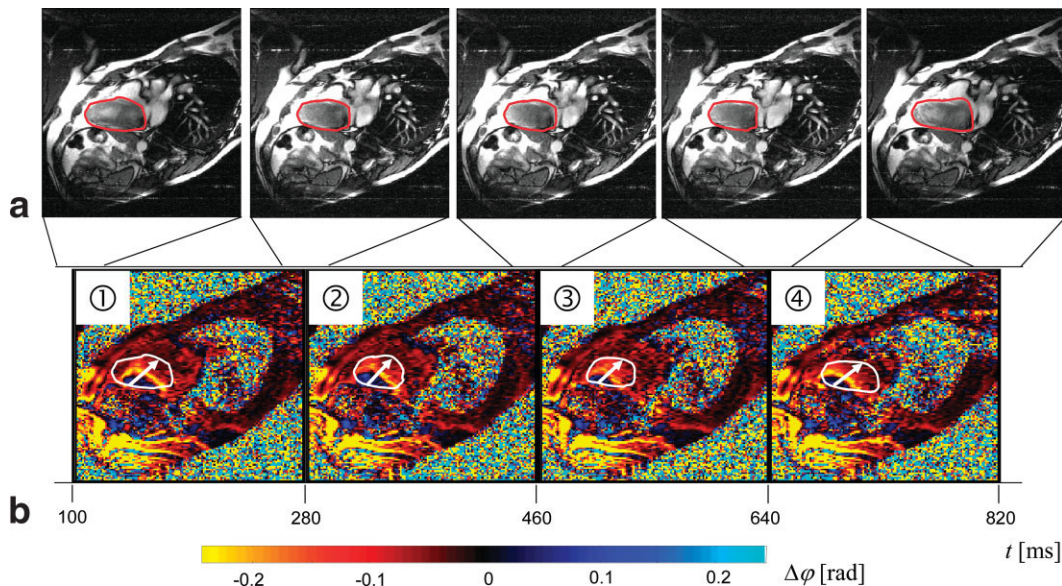


FIG. 8. Transmural wave in the IVS of a volunteer externally induced by 50-Hz vibrations of the chest. **a**: cine bSSFP-MR images for anatomical reference. The position of the IVS is demarcated by the red line. In this region the myocardium remains within the image plane of 5-mm thickness. **b**: Real part of the complex phase-difference contrast images with approximately 180-ms temporal resolution showing the externally induced vibration in the IVS ($u \approx 40$ μ m). White arrows indicate the direction of wave propagation that is visible in animations that correspond to each phase image and are provided.

pendency of the elasticity on the plate thickness (22). The thickness of the septum varied between 7 and 16 mm from late diastole to systole, which correlates to elasticities between 27 and 5 kPa, respectively. These values represent initial estimations of the expected range of elasticities in the living human heart septum. Recent results of other investigators (42,43) also indicate a wide range in the elasticity of the IVS, which underscores the need for further research.

In summary, fractional MRE provides a rapid means of mechanically testing soft and viscous materials combined with short T_2 relaxation times. It was theoretically shown that fractional motion encoding can double the accumulated motion phase in liver-like materials. The proposed fractional bSSFP-MRE experiment can be run on liver within a few breath-holds. In muscle tissue the benefit of fractional motion encoding is lower in terms of phase signal gain; however, a 10-fold acceleration of elastographic studies can be achieved compared to standard gradient-echo MRE methods (37). In the presence of blood flow or heart motion, the proposed technique enables the detection of specific components of externally introduced shear vibrations. Thus, fractional MRE uniquely provides a method for in vivo myocardial MRE.

REFERENCES

- Fung Y. Biomechanics: mechanical properties of living tissue. New York: Springer-Verlag; 1993.
- Sarvazyan AP, Skovoroda AR, Emelianov SY, Fowlkes JB, Pipe JG, Adler RS, Buxton RB, Carson PL, editors. Biophysical bases of elasticity imaging. Vol. 21. New York: Plenum Press; 1995. p 223–240.
- Ophir J, Cespedes I, Ponnekanti H, Yazdi Y, Li X. Elastography: a quantitative method for imaging the elasticity of biological tissues. *Ultrason Imaging* 1991;13:111–134.
- Parker KJ, Huang SR, Musulin RA, Lerner RM. Tissue response to mechanical vibrations for “sonoelasticity imaging.” *Ultrasound Med Biol* 1990;16:241–246.
- Muthupillai R, Lomas DJ, Rossman PJ, Greenleaf JF, Manduca A, Ehman RL. Magnetic resonance elastography by direct visualization of propagating acoustic strain waves. *Science* 1995;269:1854–1857.
- Plewes DB, Betty I, Urchuk SN, Soutar I. Visualizing tissue compliance with MR imaging. *J Magn Reson Imaging* 1995;5:733–738.
- Lewa CJ, De Certaines JD. Viscoelastic property detection by elastic displacement NMR measurements. *J Magn Reson Imaging* 1996;6:652–656.
- Chenevert TL, Skovoroda AR, O'Donnell M, Emelianov SY. Elasticity reconstructive imaging by means of stimulated echo MRI. *Magn Reson Med* 1998;39:482–490.
- Van Houten EE, Paulsen KD, Miga MI, Kennedy FE, Weaver JB. An overlapping subzone technique for MR-based elastic property reconstruction. *Magn Reson Med* 1999;42:779–786.
- Sinkus R, Lorenzen J, Schrader D, Lorenzen M, Dargatz M, Holz D. High-resolution tensor MR elastography for breast tumour detection. *Phys Med Biol* 2000;45:1649–1664.
- Weaver JB, Van Houten EE, Miga MI, Kennedy FE, Paulsen KD. Magnetic resonance elastography using 3D gradient echo measurements of steady-state motion. *Med Phys* 2001;28:1620–1628.
- Sack I, McGowan CK, Samani A, Luginbuhl C, Oakden W, Plewes DB. Observation of nonlinear shear wave propagation using magnetic resonance elastography. *Magn Reson Med* 2004;52:842.
- Othman SF, Xu H, Royston TJ, Magin RL. Microscopic magnetic resonance elastography (microMRE). *Magn Reson Med* 2005;54:605–615.
- Romano AJ, Abraham PB, Rossman PJ, Bucaro JA, Ehman RL. Determination and analysis of guided wave propagation using magnetic resonance elastography. *Magn Reson Med* 2005;54:893–900.
- McCracken PJ, Manduca A, Felmlee J, Ehman RL. Mechanical transient-based magnetic resonance elastography. *Magn Reson Med* 2005;53:628–639.
- Papazoglou S, Braun J, Hamhaber U, Sack I. Two-dimensional wave-form analysis in MR elastography of skeletal muscles. *Phys Med Biol* 2005;50:1313–1325.
- Sinkus R, Tanter M, Catheline S, Lorenzen J, Kuhl C, Sondermann E, Fink M. Imaging anisotropic and viscous properties of breast tissue by magnetic resonance-elastography. *Magn Reson Med* 2005;53:372–387.
- Overall WR, Nishimura DG, Hu BS. Fast phase-contrast velocity measurement in the steady state. *Magn Reson Med* 2002;48:890–898.
- Park JB, Olcott EW, Nishimura DG. Rapid measurement of time-averaged blood flow using ungated spiral phase-contrast. *Magn Reson Med* 2003;49:322–328.
- Markl M, Alley MT, Pelc NJ. Balanced phase-contrast steady-state free precession (PC-SSFP): a novel technique for velocity encoding by gradient inversion. *Magn Reson Med* 2003;49:945–952.
- Grinstead J, Sinha S. In-plane velocity encoding with coherent steady-state imaging. *Magn Reson Med* 2005;54:138–145.
- Graff KF. Wave motions in elastic solids. New York: Dover Publications; 1991.
- Oppelt A, Graumann R, Barfuss H, Fischer H, Hartl W, Schajor W. FISP—a new fast MRI sequence. *Electromedica* 1986;54:15–18.
- Gyngell ML. The application of steady-state free precession in rapid 2DFT NMR imaging—fast and CE-fast sequences. *Magn Reson Imaging* 1988;6:415–419.
- Patz S. Some factors that influence the steady-state in steady-state free precession. *Magn Reson Imaging* 1988;6:405–413.
- Zur Y, Wood ML, Neuringer LJ. Motion-insensitive, steady-state free precession imaging. *Magn Reson Med* 1990;16:444–459.
- Scheffler K. A pictorial description of steady-states in rapid magnetic resonance imaging. *Concepts Magn Reson* 1999;11:291–304.
- Bieri O, Maderwald S, Ladd ME, Scheffler K. Balanced alternating steady-state elastography. *Magn Reson Med* 2006;55:233–241.
- Carr HY. Steady-state free precession in nuclear magnetic resonance. *Phys Rev* 1958;112:1693–1701.
- Scheffler K, Lehnhardt S. Principles and applications of balanced SSFP techniques. *Eur Radiol* 2003;13:2409–2418.
- Wood ML, Henkelman RM. MR image artifacts from periodic motion. *Med Phys* 1985;12:143–151.
- Oliphant TE, Manduca A, Ehman RL, Greenleaf JF. Complex-valued stiffness reconstruction for magnetic resonance elastography by algebraic inversion of the differential equation. *Magn Reson Med* 2001;45:299–310.
- Catheline S, Gennisson JL, Delon G, Fink M, Sinkus R, Abouelkaram S, Culioli J. Measuring of viscoelastic properties of homogeneous soft solid using transient elastography: an inverse problem approach. *J Acoust Soc Am* 2004;116:3734–3741.
- Papazoglou S, Rump J, Braun J, Sack I. Shear-wave group-velocity inversion in MR elastography of human skeletal muscle. *Magn Reson Med* 2006;56:489–497.
- Bernstein MA, King KF, Zhou XJ. Handbook of MRI pulse sequences. Burlington: Elsevier Academic Press; 2004.
- Plewes DB, Silver S, Starkoski B, Walker CL. Magnetic resonance imaging of ultrasound fields: gradient characteristics. *J Magn Reson Imaging* 2000;11:452–457.
- Sack I, Bernarding J, Braun J. Analysis of wave patterns in MR elastography of skeletal muscle using coupled harmonic oscillator simulations. *Magn Reson Imaging* 2002;20:95–104.
- Klatt D, Asbach P, Rump J, Papazoglou S, Somasundaram R, Modrow J, Braun J, Sack I. In vivo determination of hepatic stiffness using steady-state free precession MR elastography. *Invest Radiol* 2006;41:841–848.
- Lemke AJ, Brinkmann MJ, Schott T, Niehues SM, Settmacher U, Neuhaus P, Felix R. Living donor right liver lobes: preoperative CT volumetric measurement for calculation of intraoperative weight and volume. *Radiology* 2006;240:736–742.
- Weaver JB, Qin X, Doyley MM, Van Houten EE, Kennedy FE, Paulsen KD. Encoding harmonic motion in MR elastography using the imaging gradients. In: Proceedings of the 11th Annual Meeting of ISMRM, Toronto, Canada, 2003 (Abstract 1077).
- Grimm RC, Kugel JL, Ehman RL. Improved phase to noise ratio for short T_2^* spins in MRE. In: Proceedings of the 12th Annual Meeting of ISMRM, Kyoto, Japan, 2004 (Abstract 572).
- Kanai H. Propagation of spontaneously actuated pulsive vibration in human heart wall and in vivo viscoelasticity estimation. *IEEE Trans Ultrason Ferroelectr Freq Control* 2005;52:1931–1942.
- Wen H, Bennett E, Epstein N, Plehn J. Magnetic resonance imaging assessment of myocardial elastic modulus and viscosity using displacement imaging and phase-contrast velocity mapping. *Magn Reson Med* 2005;54:538–548.